Citation: Optical Materials Express Vol. 11, Issue 6, pp. 1678-1691 (2021)

https://doi.org/10.1364/OME.424742

Optimization of the deposition parameters of MgF_2/LaF_3 narrowband reflective FUV multilayers

Paloma López-Reyes,[1,*] Belén Perea-Abarca,[1,2], Carlos Honrado-Benítez,[1] Nuria Gutiérrez-Luna,[1] Álvaro Ríos-Fernández[1], Luis V. Rodríguez-de Marcos,[1,3] and Juan I. Larruquert[1,4]

[1]*GOLD-IO-CSIC Instituto de Óptica –Consejo Superior de Investigaciones Científicas, Serrano 144, 28006 Madrid, Spain*
[2]*LABMET–Universidad Carlos III de Madrid, Av. de la Universidad, 30, 28911 Leganés, Madrid, Spain.*
[3]*Catholic University of America and NASA Goddard Space Center (CRESST II), Greenbelt, MD 20771, USA*
[4]*j.larruquert@csic.es*
**paloma.lopez@csic.es*

Abstract: The development of efficient dielectric coatings in the far UV (FUV) is demanded for upcoming space instrumentation, such as LUMOS (LUVOIR Ultraviolet Multi-Object Spectrograph) in LUVOIR mission, among other applications. Multilayers (MLs) based on MgF_2 and LaF_3 have been developed in the last decades for the 157-nm and 193-nm lithography, demonstrating excellent optical properties. Yet, the deposition procedure to obtain coatings with optimal performance has not been fully detailed in the open literature, such as the dependence of ML performance with deposition and post-deposition temperature. This research investigates the effect of the substrate deposition temperature of MgF_2/LaF_3 ML coatings prepared by thermal evaporation on FUV reflectance, stress, roughness, as well as the performance of the coatings and their evolution over time. The relatively higher expansion coefficient of these two fluorides in comparison with fused silica substrates results in a large tensile stress for coatings deposited at high temperature and later cooled down to room temperature. Such stress may result in coating cracking and delamination. A compromise deposition temperature of ~240ºC and 13 bilayers was found for optimal ML reflectance peaked at ~160 nm before cracks are generated. Above this deposition temperature, stress increased, which resulted in an extension of the cracked area and in a slight roughness increase and FUV reflectance decrease. MLs that were deposited at room temperature and later annealed resulted in a similar reflectance and stress to those of hot-deposited coatings for a given temperature.

1. Introduction

Astronomical observations in the far ultraviolet (FUV; λ=100-200 nm) are key to unveil fundamental information for astrophysics, solar physics and atmosphere physics. FUV contains a wealth of spectral lines with a unique diagnostic potential for the physics of the local Universe. FUV astronomy has been heavily hindered by optical-coating performance, along with detectors, which ultimately limit the sensitivity of space telescopes and their instruments. The high absorption of materials and the need of an accurate knowledge of their optical constants in this part of the spectrum are among the chief factors that limit coating optical performance [1].

Future space missions will require efficient FUV coatings. LUVOIR is a large mission concept to cover the FUV that competes to become the next NASA flagship mission. Among the sub-assemblies proposed in LUVOIR, LUMOS (LUVOIR Ultraviolet Multi-Object

Spectrograph) will offer point source and multi-object spectroscopy across the UV bandpass. It will provide, among others, low and medium resolution modes across the FUV and near-ultraviolet observation windows. LUMOS instrument is being designed to support LUVOIR UV science requirements, from exoplanet host star characterization to tomography of circumgalactic halos and to water plumes on outer solar system satellites [2]. LUMOS includes a FUV imaging channel that will employ narrow- and medium-band filters. The International Solar-Terrestrial Physics (ISTP) was a pioneering instrument to include FUV narrowband coatings [3]. Considering that LUMOS has been envisioned to explore very faint objects in the FUV, coatings with enhanced performance are desired. Other fields may benefit from the development of more efficient FUV bandpass mirrors, from space observations for solar physics and atmosphere physics to other fields that involve FUV radiation, such as excimer laser optics, petawatt-laser beamlines, thermonuclear fusion reactors and the semiconductor industry.

FUV reflective filters are based on multilayers (MLs) of two low absorption materials with high- and low-refractive indices in Bragg configuration [4,5]. Fluorides are the materials of choice for these MLs, as they are the materials that keep their transparency deeper in the FUV. LiF is the material in nature with the shortest cutoff of ~102 nm; however, LiF hygroscopic nature complicates its practical application [6]. MgF_2 is the next material with shortest cutoff at 115 nm, except for AlF_3, a material with similar FUV properties to MgF_2, but short on experience. MgF_2 is a very prominent fluoride due to its low refractive index over a wide spectral range from the FUV to the mid-IR as well as low absorption and acceptable mechanical robustness. The second material in the ML must be also as transparent as possible and must have a contrasting refractive index with MgF_2. LaF_3 has been most often chosen as the high-index material. GdF_3 is a secondary high-index material choice, but it is expected to have a somewhat longer cutoff compared to LaF_3.

FUV ML coatings of MgF_2/LaF_3 are better deposited by evaporation in vacuum. However, coatings deposited via evaporation grow with large porosity when deposited on a substrate at room temperature (RT). Such porosity could be filled with water vapour molecules or other contaminants upon exposure to the atmosphere, which may increase FUV radiation absorption and hence decrease coating performance.

Fluoride films coated by evaporation are known to be more transparent in the FUV when deposited on a hot substrate [7]. This extra transparency in each layer is expected to provide a ML with enhanced reflectance. Evaporation-deposited fluoride coatings that grow on a hot substrate typically develop high tensile stress, which may cause the optics to deform and even coating cracking or delamination. For MLs of fluorides, this tensile stress is mostly due to a large thermal expansion coefficient difference between the substrate and the film materials when coatings are deposited at high temperatures on low expansion substrates, such as fused silica or Zerodur®. A trade-off between the number of bilayers, deposition temperature and stress needs to be determined.

ML coatings based on MgF_2 and LaF_3 have been reported in the literature [**3**,8,9,10,11,12,13]. Yet the deposition procedure to obtain coatings with optimal performance has not been fully detailed in the open literature, such as the dependence of ML performance with deposition and post-deposition temperature.

The objective of the present study is to optimize the main deposition parameters of high-reflectance FUV filters tuned at approximately 160 nm as an archetype that can be tailored to peak the ML at any FUV wavelength longwards of ~120 nm, such as the various filters proposed for LUMOS [**2**]. The present MLs, that peak at 160 nm, could be also applicable to optical systems that involve an F_2 excimer laser, operating at the close 157 nm wavelength, among other applications.

The influence of the number of layers in MgF_2/LaF_3 MLs and its deposition and/or post-deposition temperature on optical performance, mechanical robustness and coating durability has been investigated. The present research is organized as follows. Section 2 describes the experimental techniques used. Sections 3 and 4 present the results obtained on the dependence of deposition and post-deposition temperature on ML reflectance, stress, roughness and cracks and a discussion about these results. By evaluating both the design and the deposition temperature, this research provides an optimization of the main deposition parameters of MgF_2/LaF_3 MLs prepared by thermal evaporation to obtain good performing, stable and durable coatings tuned in the FUV.

2. Experimental

MgF_2/LaF_3 MLs were deposited in a high-vacuum chamber pumped with a turbo-Roots pump system and a Ti sublimation pump with a shroud that is cooled down with liquid N_2. VUV-grade MgF_2 and 99.99% pure LaF_3 were evaporated from W boats with deposition rates of ~0.9 nm/s for MgF_2 and ~0.4 nm/s for LaF_3. Chamber base pressure was 3×10^{-5} Pa and it increased to $\sim3\times10^{-4}$ Pa during deposition. Film thickness was measured in situ with a quartz-crystal monitor that had been previously calibrated by profilometry. The total coating thickness was measured with contact profilometry and/or by fitting reflectance and/or ellipsometry measurements.

The ML was deposited on a substrate in contact with a resistance heater; two K thermocouples were used to measure temperature. Coatings were deposited onto 2”-diameter, 0.5 mm-thick, two-side polished fused silica (FS) wafers, with a root-mean-square (RMS) roughness of less than 1 nm. Substrates were cleaned through several rinses with organic solvents and with a glow discharge in vacuum. FS was selected because it is a common and accessible substrate material for optics, even though its thermal expansion coefficient contrasts starkly with the expansion coefficient of the fluorides of the coating. Substrate temperature was stabilized for ~1-2 h before deposition to favour uniformity. When deposition was finished, the coating was cooled down at a rate of ~0.3ºC/min. A slow cooling has proved to be successful to slightly reducing stress in MgF_2/LaF_3 mirrors [12]. Various samples were deposited at RT or at a relatively low temperature and annealed in vacuum *in situ*.

Stress was measured *ex situ* at RT by the curvature method using a contact profilometer which was adapted to guarantee sample relocation after deposition. To avoid external loads that could affect the macroscopic stress during deposition, a “free-tension” holder was designed to place the wafers in contact with the heating element. The radius of curvature was measured in two perpendicular directions before and after deposition. Stress was calculated by averaging both measurements, which were obtained several times to reduce uncertainty. Error propagation of the relevant parameters was performed to estimate stress error.

The optical surface quality regarding the growth of cracks and/or delamination caused by stress and the presence of particles deposited in the evaporation process was evaluated with an optical microscope in dark field mode, checking the whole surface with different magnifications.

FUV fluoride ML reflectance was measured in GOLD’s reflectometer (GOLD is the Spanish acronym for Thin Films Optics Group, Madrid, Spain), which operates in ultra-high vacuum (UHV) conditions. The reflectometer has a grazing-incidence, toroidal-grating monochromator, with entrance and exit arms 146º apart, which covers the 12.5-200 nm

spectral range. A deuterium lamp was used to cover a range of 113 to 185 nm. A channel-electron-multiplier with a CsI-coated photocatode was used as a light detector. Reflectance was obtained by alternately measuring the incident intensity and the intensity of the light beam reflected by the sample. Reflectance measurements were performed at 5º from normal incidence. FUV reflectance was initially measured after ~one-hour sample contact with the atmosphere, which will be referred to as fresh and it was also measured after various months of storage in a desiccator. Some aged samples were measured at NASA Goddard Space Flight Centre (GSFC) with a McPherson Vacuum Ultraviolet (VUV) 225 spectrophotometer. This spectrometer has a one-meter length, high-vacuum monochromator with a 1200 lines/mm grating at near-normal incidence operating in the spectral range from 30 nm to 325 nm. The spectrometer is equipped with a windowless hydrogen-purged light source, which provides discrete H_2 emission lines between 90 nm and 160 nm and a continuum above these wavelengths. The detector, which is housed inside a sample-holder compartment, consists of a photomultiplier cathode tube connected to a light-pipe for feeding the light signal coming out of the monochromator. The light pipe has a fluorescence and high quantum efficiency coating of sodium salicylate that is used to convert the FUV radiation into visible light. Reflectance measurements with the latter spectrophotometer were performed at 10° from normal incidence; a negligible reflectance difference from normal incidence to 10º is calculated for the present MLs.

AFM analysis of microroughness was performed with a height resolution scanning probe microscope in tapping mode. The tip radius was 20 nm. AFM images of 1 x 1 μm were obtained.

3. Results

3. 1. Design optimization

A preliminary study was made to define a suitable design for a $(HL)^n$ periodic ML, where MgF_2 is the low index material (L), LaF_3 is the high index material (H) and *n* is the number of bilayers. Nominal layer thicknesses of 28.1 nm (MgF_2) and 21.1 nm (LaF_3) were used in a quarterwave (QW) ML design [5] using the optical constants of the two fluorides reported in the literature [13].
Several MgF_2/LaF_3 ML mirrors peaked at ~160 nm with different number of layer pairs ranging from 12 to 21 were deposited on glass substrates at 250ºC, the reported MgF_2 optimal deposition temperature for broadband Al/MgF_2 mirrors [14].
The large stress of fluoride coatings deposited on substrate materials with low thermal expansion coefficient may result in coating cracking and delamination. It has been reported that these cracks and delamination in MLs are correlated with the force per unit width (FPUW) more than with total stress [15,16]. FPUW equals the integral of total stress through ML film thickness; assuming that stress does not vary with film thickness, FPUW equals stress times film thickness [15,16]. According to this, FPUW is proportional to the number of bilayers, for a constant bilayer thickness, so that there must be a bilayer number threshold above which cracks and/or delamination are typically produced. The coatings were observed by optical microscopy and cracks were noticed on coatings above 14 layer pairs, whereas no cracks were observed for coatings with 13 and 12 bilayers. Let us see the effect of the number of bilayers on reflectance. Figure 1 a) compares the reflectance measured for MLs with 13 and 15 bilayers. No significant difference on peak reflectance was obtained. Fig. 1 b) presents the calculated percentage of maximum peak reflectance as a function of the number of bilayers. Calculations were performed with MgF_2 and LaF_3 optical constants obtained for films deposited at 250ºC [14]. Roughness was assumed to increase with total thickness as in [16]. In the calculations, the effect of cracks or delamination was not considered. By limiting

the ML to 13 bilayers, reflectance could be at most of 4% below the theoretical maximum, whereas between 13 and 15 bilayers such difference stays below 2%. This is due to a modest reflectance increase per added bilayer above a reasonable number of bilayers, along with the trend of surface and interface roughness to grow with the number of layers [17,18]. In most practical situations, a reflectance close to maximum with no cracks in the coating is expected to be the best choice. Hence the design chosen was periodic MLs with n=13 bilayers, around the threshold of cracking appearance while maintaining low scatter losses.

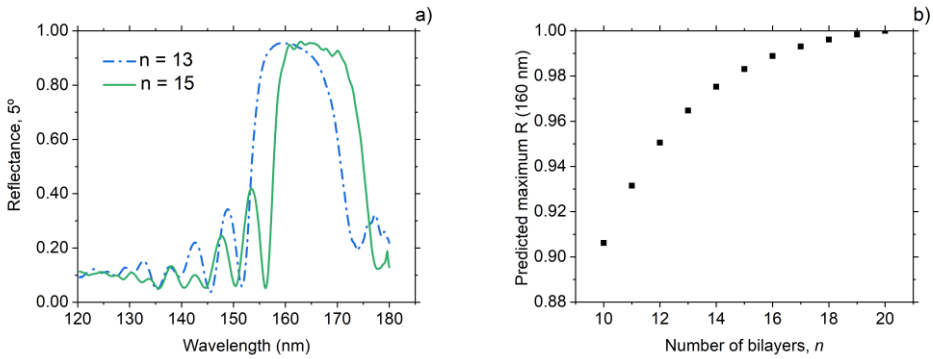

Fig. 1. a) Fresh reflectance as a function of wavelength of $(MgF_2/LaF_3)^n$ filters deposited onto **glass** substrates at 250ºC for two different numbers of layer pairs, *n*. b) Calculated peak reflectance as a function of *n* for $(MgF_2/LaF_3)^n$ filters taking into account the increasing roughness with thickness.

3.2 Temperature effect

A set of nine narrowband reflectors nominally tuned at 160 nm were deposited on FS substrates at temperatures ranging from RT to 400ºC. Additionally, three samples were deposited at RT or at a relatively low substrate temperature and later annealed in vacuum over a period of 2-3 hours. The purpose of the latter samples was to compare post-annealing with hot deposition. The design was nominally the same for all samples, with periodic bilayers and n = 13. The nominal thicknesses were 28.1 nm (MgF_2) and 21.1 nm (LaF_3). Table 1 highlights the relevant deposition parameters for the different samples.

Table 1. Deposition or post-deposition temperatures

Sample Name	Deposition Temperature (ºC)	Post-annealing treatment (ºC)
M45	45ºC	-
M80	80ºC	-
M240	240ºC	-
M240_2	240ºC	-
M300	300ºC	-
M400	400ºC	-
M50A240	50ºC	240ºC
M50A240_2	50ºC	240ºC
M100A240	100ºC	240ºC

Fig. 2 displays the reflectance of several samples deposited at various temperatures both fresh and aged from 1 to 10 months in a desiccator. An increasing deposition temperature is expected to increase each material density and to vary its refractive index too [7,19], which results in that the correct film thickness and mass of MgF_2 and LaF_3 layers depend on the deposition temperature. Even though we attempted to counteract such dependence through slight film thickness adaptation to obtain coatings peaked at 160 nm, there was some

dispersion in ML peak. Central wavelength λ_0, peak reflectance $R(\lambda_0)$ and bandwidth (FWHM) of fresh and aged ML coatings are compared in table 2 for the samples shown in Fig 2.

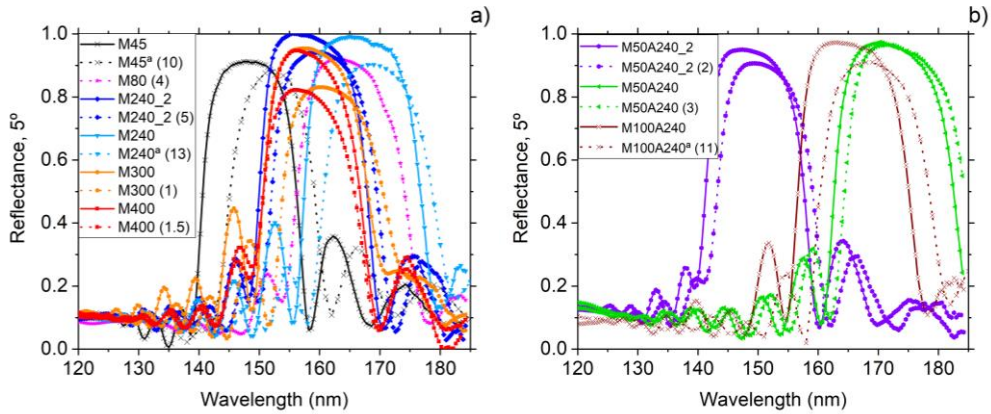

Fig. 2. Reflectance as a function of wavelength of fresh and aged (MgF_2 /LaF_3)[13] filters at different deposition (a) or annealing temperatures (b). Ageing period in months is shown in parenthesis. Solid (dotted) lines correspond to fresh (aged) measurements. ªM45 (45ºC), M240 (240ºC) and M100A240 (100ºC + 240ºC ann.) ~1 year aged samples were measured at NASA/GSFC.

Central wavelength λ_0, peak reflectance $R(\lambda_0)$ and bandwidth (FWHM) of fresh and aged multilayer coatings are compared in Table 2 for the samples shown in Fig 2.

Table 2. Central wavelength, reflectance at central wavelength, FWHM, and stress of fresh and aged samples

Deposition Temperature (T_d °C)	λ_0 (nm) Fresh/Aged	$\bar{R}$ (λ_0) Fresh/Aged	FWHM (nm) Fresh/Aged	Stress (MPa) Fresh/Aged
M45 (45ºC)	148.4 / 152.1	0.91 / 0.88	15.9 / 14.6	84.5 / -
M80 (80ºC)	- / 165.2	- /0.91	- / 18.3	137 / 89.5
M240 (240ºC)	167 / 169.8	0.98 / 0.90	19.3 / 18.6	137 / 77.5
M240_2 (240ºC)	159 / 160.8	0.99 / 0.93	17.9 / 17.5	170 / 112
M300 (300ºC)	159.4 / 162.5	0.94 / 0.82	17.8 / 17.8	217 / 110
M400 (400ºC)	158.4 /158.2	0.93 / 0.81	16.6 /16.2	292 / 263
M50A240 (50ºC + 240ºC A)	172.6 /174.2	0.96 / 0.94	20 / -	147.5 / 67.5
M50A240_2 (50ºC + 240ºC A)	149.4 / 151.6	0.94 / 0.90	16.6 /16.3	140.5 / 55.5
M100A240 (100ºC + 240ºC A)	165.8 / 169.4	0.96 / 0.91	18.6 /18.7	137 / -

3.3 Stress

The total stress of a thin film can be decomposed into various contributions that are related with microstructure, chemical reactions, external loads and thermal changes [20]. Among these components, thermal stress is caused by the difference in thermal expansion coefficients (CTE) between the substrate (α_{sub}) and the film (α_{film}) and by the temperature difference between deposition (T_d) and stress measurement (T) [15,21]:

$$\sigma_{therm} = \left(\frac{E}{1-\nu}\right)_{film} \left(\alpha_{sub} - \alpha_{film}\right)(T - T_d) \quad (1)$$

where E and ν stand for Young modulus and Poisson ratio of the coating, respectively and $(E/1-\nu)_{film}$ is called the biaxial modulus of the coating. Both CTE and biaxial modulus depend on the coating microstructure and may deviate from the bulk material. The present MLs (except for the RT one) are assumed to involve mostly thermal stress induced by the large expansion-coefficient difference between the fluorides and the substrate [15,22].

Coating stress causes a curvature change on the substrate, which can be measured to calculate the film stress. If substrate thickness, d_s, is large compared to film thickness, d_f, the total stress, σ_{total}, is given by Stoney's equation, which relates the total, macroscopic stress with the change in the substrate radii before (R_0) and after (R_d) deposition [23]:

$$\sigma_{total} = \frac{E}{1-\nu}\frac{d_s^2}{6d_f}\left(\frac{1}{R_d}-\frac{1}{R_0}\right) \quad (2)$$

Stoney's equation can be generalized to MLs, assuming that each individual layer contributes to the total deformation of the substrate regardless of its position and of its neighbours [24,25]. The stress measured for the present samples is displayed in table 2 and in Fig. 3 a). Fig. 3 b) displays stress relaxation over time for samples stored in a desiccator.

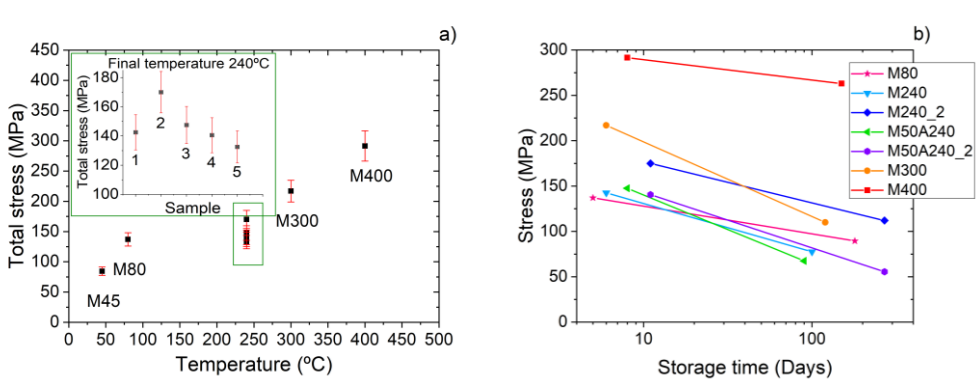

Fig. 3. a) Total stress vs deposition or annealing temperature for samples presented in table 1. The numbers in the inset refer to samples (1) M240, (2) M240_2, (3) M50A240, (4) M50A240_2 and (5) M100A240. b) Sample stress relaxation over time.

3.4 Optical Microscopy

Coatings were inspected through optical microscopy to evaluate the density of cracks and/or the presence of delamination. Images were taken after few hours of contact with the atmosphere and they were taken again several months after deposition on similar sample areas. Fig. 4 displays dark-field optical microscopy images taken after few hours contact with the atmosphere for samples deposited at a) 45ºC, b) 240ºC, c) 400ºC and d) for the sample deposited at 50ºC and annealed at 240ºC. Fig. 5 displays dark-field optical microscopy images of the sample deposited at 400ºC a) after few hours of contact with the atmosphere, b) after ~one year stored in a desiccator.

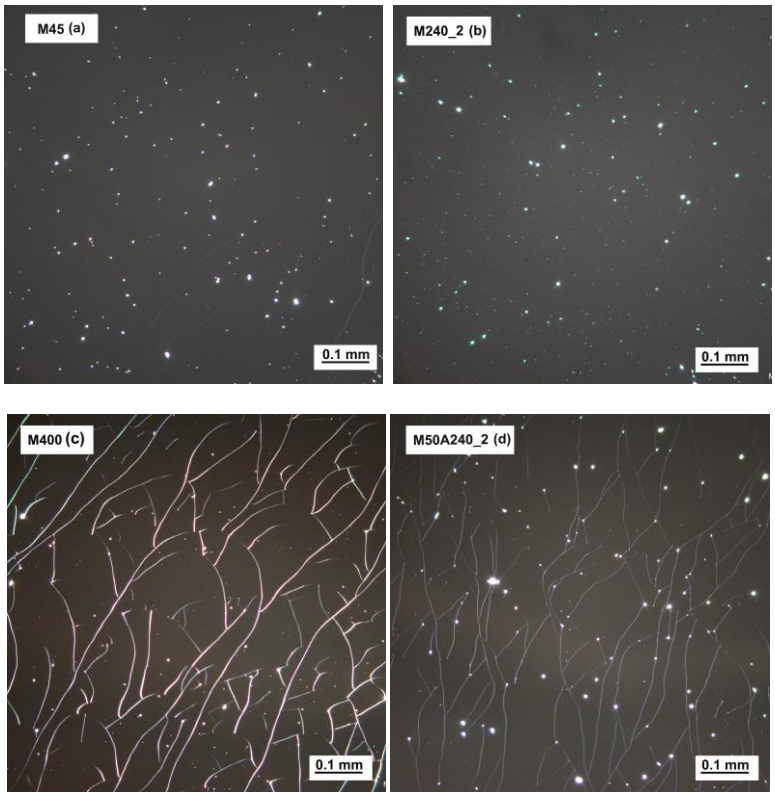

Fig.4. Dark-field images of $(MgF_2/LaF_3)_{13}$ MLs on FS deposited at 45ºC (M45) (a), 240ºC (M240) (b), 400ºC (M400) (c) and 50ºC + annealing at 240ºC (M50A240_2) (d). Images were taken after few hours contact with the atmosphere.

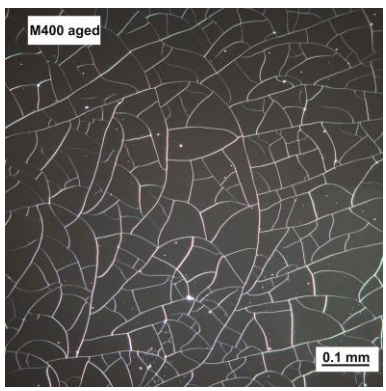

Fig.5. Dark-field image of $(MgF_2/LaF_3)_{13}$ ML on FS deposited at 400ºC (M400) after ~1 year stored in a desiccator. The image corresponds to an area similar to the area in Fig. 4 c)

3.5 Topography

Surface topography was measured for various samples with AFM to calculate surface roughness. Fig. 6 displays the resulting topography of the analyzed surfaces.

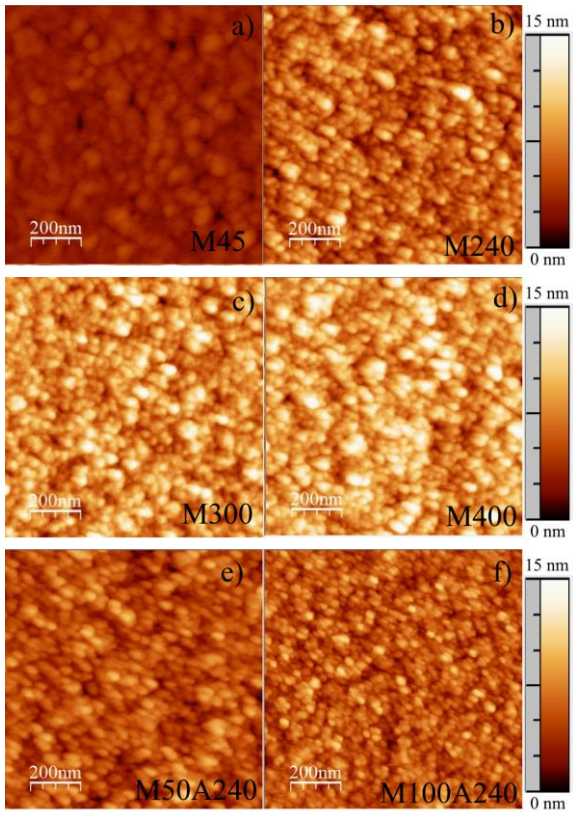

Fig.6 Surface topography of $(MgF_2/LaF_3)_{13}$ MLs on FS deposited at 45ºC (M45) (a), 240ºC (M240) (b), 300ºC (M300) (c), 400ºC (M400) (d), 50ºC + annealing at 240ºC (M50A240) and 100ºC + annealing at 240ºC (M100A240)

From AFM data, Power Spectral Density (PSD) curves were calculated, which are plotted in Fig. 7. PSD provides information about the contributions of the different spatial frequencies to surface roughness. Table 3 displays RMS roughness for samples deposited and/or post-annealed at different temperatures.

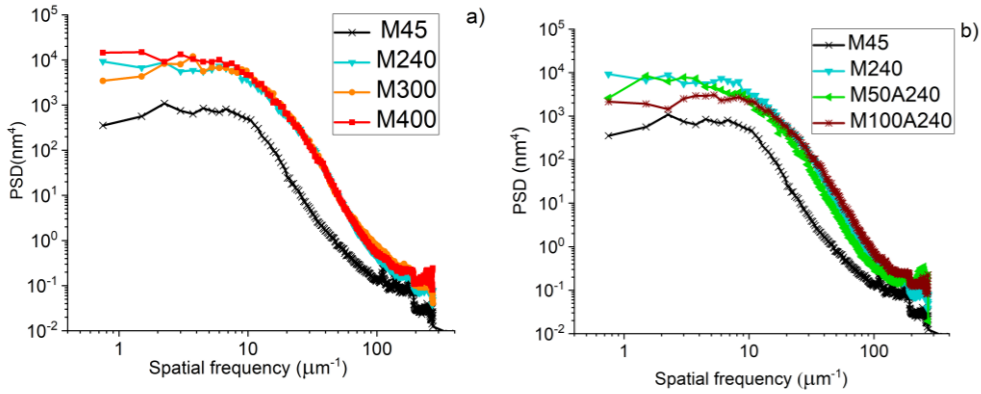

Fig.7. Power Spectral Density calculated from AFM images for various samples.

RMS roughness, R_q, was calculated by integrating PSD through the frequency spectrum covered and is presented in table 3

Table 3. RMS roughness for samples deposited at different temperatures ranging from 45ºC to 400ºC and for post-annealed samples.

Sample Name	M45	M240	M50A240	M100A240	M300	M400
R_q (nm)	0.6	2.0	1.6	1.7	2.1	2.2

4. Discussion

4.1 Fresh coatings

The largest reflectance was obtained for ML coatings deposited at 240°C. This temperature is consistent with the optimum deposition temperature found for MgF_2 protective layer on Al for broadband FUV mirrors [14]. For the latter coatings, a trade-off is necessary between the increasing transparency of MgF_2 with deposition temperature [14] and the increasing Al roughness with temperature. In the present case, a trade-off must be found between the increased transparency of the fluorides with temperature and their increase of stress and surface roughness both with temperature and with the number of layers or total coating thickness. Deposition of the fluoride layers at increased substrate temperatures result in layer density increase, which may be related with the enhanced transparency [14]. For coatings deposited at 300ºC and above, reflectance decreases. This effect may be in part due to the growth of cracks; it can also be due to the possible interdiffusion enhancement at the interfaces and, to a small extent, to the slight roughness increase with deposition temperature. For samples centered at shorter wavelengths, such as M50A240_2, a comparative lower peak reflectance when fresh may be partly attributed to the somewhat higher absorption of the fluoride layers at shorter wavelengths. A fresh reflectivity of 99% at 160 nm was measured and it kept above 90% after almost a year of ageing. These results are similar to reported values in literature [9]. Post-annealed samples reflectance was almost as high as for samples deposited on hot substrates, which suggests that the post-annealing process is also a successful procedure to increase layer transparency and hence the reflectivity of the ML coatings.

Both stress and roughness increased with deposition temperature. Roughness severely increased from RT to 240ºC but it further increased only marginally for coatings deposited at

higher temperatures. Ref. [11] shows a RMS roughness of 2.39 nm for a $(MgF_2/LaF_3)_{20}$ mirror on FS tuned at 193 nm and Ref. [16] shows values above 3 nm for ~600 nm thickness MgF_2/LaF_3 mirrors deposited at 250ºC on FS. These values are slightly higher but comparable with present results.

Stress increased with temperature quasi-linearly for this ML design, confirming that thermal stress is the main component of macroscopic stress in samples deposited on heated substrates [15,22]. The stress of post-annealed samples and of samples heated while deposited was very similar.

Fig. 4 shows that both crack width and crack density grow with deposition temperature, since both stress and hence FPUW increase with the latter. To evaluate this effect, we estimated the crack fraction area over the microscopy images. Samples with post-annealing treatment showed a larger crack density than the sample deposited directly at the same temperature. This result can be attributed to the fact that post-annealed samples undergo an expansion followed by a contraction process. Furthermore, in the post-annealing procedure the coating remained longer time at the hot temperature compared to hot-deposited samples. Cracks in samples deposited on a hot substrate were seen to be rather directional, as can be observed in the sample deposited at 400ºC. This effect is not seen in the post-annealed samples. As FS is an amorphous material, no cracking directionality is expected, so that we found no explanation for it. As seen principally in Fig. 4 d), cracks seem to begin at point defects, as they might be weaker areas. These defects are believed to be mostly particles originated from material spitting out of the evaporation boats during deposition, because they were not visible under microscopy on inspection after substrate cleaning prior to deposition. Hence minimizing particle spitting is expected to be an effective way to reduce the cracked area.

For fresh hot-deposited samples, a correlation between crack density and temperature was observed. Additionally, the smaller reflectance for temperatures above 240ºC is correlated also with the crack density increase. The latter may not explain the full losses observed on peak reflectance. The sample deposited at RT showed a lower reflectance, which is attributed to the loss of transparency due to water or contaminant absorption within its porous structure and not to crack formation. Summarizing the aforementioned studied effects, the determination of the optimal deposition temperature involves a balance between a high temperature that leads to film density closer to bulk and to increased transparency, while keeping low stress values and low crack formation.

4.2 Coating evolution over time

In addition to the decrease of reflectance, sample stress also decreased over time. Fig. 5 shows that cracking is also a dynamic process: the density of cracks grows with storage time. This behaviour had been previously observed [15]. To evaluate the effect of cracking increase, we summed up the lengths of the cracks over the microscopy images on equal areas for both fresh and aged samples and we obtained that samples with the highest initial stress (such as M300 or M400) developed more cracks during storage than samples with initially lower levels of stress.

Reflectance decay over time could be partly explained by further crack development, but there may be also some other aging phenomena, such as some possible interdiffusion processes at the layer interfaces. The absorption of some water or other contaminants either in the porous structure, which is expected to be larger for low deposition-temperature samples, or on the slightly larger effective surface provided by the enhanced roughness, which somewhat grows with deposition temperature, might be related with reflectance decay, as

well. Water absorption could be noticed in the annealed sample that was peaked at ~150 nm, which decayed twice than the annealed sample peaked at ~170 nm. Its more severe ageing is compatible with the larger extinction coefficient of water by two orders of magnitude at 150 nm compared with 170 nm [26].

The initial stress was observed to decrease over time, which is understood as a relaxation process. This behaviour was not analyzed in depth, but we propose several processes that may have contributed to such decrease. Stress decrease over time could be explained as gradual relaxation at the coating-substrate interface, where atoms tend to reach a lower energy configuration driven by atom natural vibration. In case interfaces undergo some interdiffusion, the latter might contribute to some stress relaxation. Samples coated at higher temperatures, like M400, are expected to undergo a larger interdiffusion initially and hence a smaller relaxation can be expected over time. Stress relaxation has been also associated with water absorption in the pore structure of the coating [12,16,27]. Water molecules probably reduce the electrostatic attraction forces at grain boundaries, hence reducing thermal stress. This would explain a higher relaxation through water absorption for samples deposited at lower temperatures, which are more porous and hence, would absorb more water than samples with film packing density closer to bulk. However, water absorption might be a somewhat superficial phenomenon, at least for coatings deposited at relatively high temperatures, so that its stress relaxation capacity at deep layers is presumed to be small. The generation of new cracks over time is expected to provide some stress release too, as crack generation causes some reduction on the thermally-induced mismatch between film and substrate.

The present MLs underwent a band shift over time. Hence all samples, except the sample deposited at 400ºC, underwent a reflectance shift to longer wavelengths of ~2 nm that should be taken into account in the design. This behaviour had been also observed on aged fluoride MLs [28] and has been previously reported for fluoride coatings, as a result of water or oxygen absorption [19,28]. Band-shape changes and/or band shifts can be also explained by interdiffusion of materials over time. The lack of shift for the sample deposited at 400ºC might be due to a lower porosity and to that most of the interdiffusion process might have occurred before its reflectance was measured, leaving small room for further interdiffusion over time, which would also explain the aforementioned lower stress relaxation caused by interdiffusion.

5. Conclusions

The dependence of FUV reflectance, stress, roughness and crack generation with deposition and post-deposition temperature for the preparation of optimum MgF_2/LaF_3 narrowband coatings peaked at ~160 nm has been investigated. A compromise deposition temperature of ~240°C and 13 bilayers was found for optimal reflectance before cracks are generated and it is also a good trade-off to restrain scattering losses. Fresh peak reflectance values of about 99% were achieved, while values above 90% remained after almost a year of storage in desiccator. Temperatures above 240ºC resulted in MLs with lower reflectance while roughness only slightly increased above this temperature, keeping RMS values of ~2 nm. Stress was found to approximately increase in a linear way with deposition temperature, leading to crack formation on 13-bilayer MLs, which contributed to reflectivity losses. For coatings deposited at 300°C and above, roughness only increased slightly and most of the lower reflectance at these deposition temperatures is attributed to the increase of the cracked area and possibly to enhanced interdiffusion across interfaces.

Upon sample ageing, stress displayed a trend to decrease. Final stress values of ~100 MPa were measured for samples deposited or post-annealed at 240ºC after several months of ageing. Both stress and reflectance decrease over time can be correlated with several factors, including the generation of new cracks over time, which was found to be more critical for samples that showed larger stress values initially.

The other factors that could explain the reflectance and stress losses over time are the absorption of water or other contaminants in the ML, as well as the interdiffusion between the fluorides that is seemingly to occur in the interfaces progressively over time. The interdiffusion and the absorption of contaminants might also explain the band shifts towards longer wavelengths observed in aged samples.

6. Funding, acknowledgments, and disclosures

6.1. Funding

This work was supported by the Ministerio de Economía, Industria y Competitividad, project numbers ESP2016-76591-P, BES-2017-081909, and PID2019-105156GB-I00.

6. 2. Acknowledgments

We gratefully acknowledge R. Álvaro and “Instituto de micro y nanotecnología” (CSIC) for AFM measurements, M. Vélez of “Instituto de Catálisis y Petroleoquímica” (CSIC) for her support with AFM and M. Quijada and “NASA/GSFC” for aged reflectance measurements.

6. 3. Disclosures

“The authors declare no conflicts of interest.”

7. References

1. J. Tumlinson, A. Aloisi, G. Kriss, K. France, S. McCandliss, K. Sembach, A. Fox, T. Tripp, E. Jenkins, M. Beasley, C. Danforth, M. Shull, J. Stocke, N. Lehner, C. Howk, C. Froning, J. Green, C. Oliveira, A. Fullerton, B. Blair, J. Kruk, G. Sonneborn, S. Penton, B. Wakker, X. Prochaska, J. Vallerga, and P. Scowen, "Unique Astrophysics in the Lyman Ultraviolet," https://arxiv.org/abs/1209.3272
2. K. France, B. Fleming, G. West, S. R. McCandliss, M. R. Bolcar, W. Harris, L. Moustakas, J. M. O’Meara, I. Pascucci, J. Rigby, D. Schiminovich, and J. Tumlinson, “The LUVOIR Ultraviolet Multi-Object Spectrograph (LUMOS): Instrument definition and design,” Proc. SPIE 10397, 1039713 (2017).
3. M. Zukic, D. G. Torr, J. F. Spann, and M. R. Torr, "Vacuum ultraviolet thin films 2: Vacuum ultraviolet all-dielectric narrowband filters," Appl. Opt. **29**(28), 4293-4302 (1990).
4. E. Spiller, “Interference in thin films: theory”, *Soft X-Ray Optics*, (SPIE -The International Society for Optical Engineering, 2011), pp. 101-137.
5. J. I. Larruquert, *Optical Properties of Thin Film Materials at Short Wavelengths*, A. Piegari, F. Flory, eds. (Woodhead Publishing Series in Electronic and Optical Materials, 2018).
6. D. W. Angel, W. R. Hunter, R. Tousey, and G. Hass, "Extreme Ultraviolet Reflectance of LiF-Coated Aluminum Mirrors," J. Opt. Soc. Am. **51**(8), 913-914 (1961).
7. O. R. Wood, H. G. Craighead, J. E. Sweeney, and P. J. Maloney, "Vacuum ultraviolet loss in magnesium fluoride films," Appl. Opt. **23**(20) 3644-3649 (1984).
8. H. Bernitzki, H. Lauth, R. Thielsch, H. Blaschke, N. Kaiser, and K. R. Mann, "Current status of radiation resistance of dielectric mirrors in the DUV," Proc. SPIE 3578, 105-116 (1999).
9. R. Thielsch, "Optical coatings for the DUV / VUV," in *Optical Interference Coatings*, N. Kaiser; H.K. Pulker, eds. (Springer, 2003), pp. 257–277.
10. J. E. Rudisill, A. Dupparre, and S. Schroeder, "Determination of scattering losses in ArF* excimer laser all-dielectric mirrors for 193 nm microlithography application," Proc. SPIE 5647, 9-22 (2005).

11. S. Günster, D. Ristau, A. Gatto, N. Kaiser, M. Trovó, and M. Danailov, "Storage ring free-electron lasing at 176 nm-dielectric mirror development for vacuum ultraviolet free-electron lasers," Appl. Opt. **45**(23), 5866-5870 (2006).
12. G. hui Liu, Q. ling Xiao, Y. xia Jin, W. li Zhang, H. bo He, and Z. xiu Fan, "Mechanical stress in 355 nm LaF3/MgF2 high reflectors with various layer-pair number and methods for reduction," Vacuum **84**(6), 778–781 (2010).
13. L. Rodríguez-de Marcos, J. I. Larruquert, J. A. Méndez, and J. A. Aznárez, "Multilayers and optical constants of various fluorides in the far UV," Proc. SPIE 9627, 96270B (2015).
14. L. V. R. De Marcos, J. I. Larruquert, J. A. Méndez, N. Gutiérrez-Luna, L. Espinosa-Yáñez, C. Honrado-Benítez, J. Chavero-Royán, and B. Perea-Abarca, "Optimization of MgF_2 –deposition temperatura for far UV Al mirrors," Opt. Express **26**(7) 9363-9372 (2018).
15. J. Ullmann, H.-G. Keck, R. Thielsch, H. Uhlig, and N. Kaiser, "Mechanical stress in fluoride coatings," Proc. SPIE 3738, 136-147 (1999).
16. R. Thielsch, J. Heber, H. Uhlig, and N. Kaiser, "Development of mechanical stress in fluoride multilayers for UV applications," Proc. SPIE 5250, 127-136 (2004).
17. D. Ristau, S. Günster, S. Bosch, A. Duparré, E. Masetti, J. Ferré-Borrull, G. Kiriakidis, F. Peiró, E. Quesnel, and A. Tikhonravov, "Ultraviolet optical and microstructural properties of MgF_2 and LaF_3 coatings deposited by ion-beam sputtering and boat and electron-beam evaporation," Appl. Opt. **41**(16), 3196-3204 (2002).
18. S. Schröder, H. Uhlig, A. Duparré, N. Kaiser, F. Angewandte, and D.- Jena, "Nanostructure and optical properties of fluoride films for high-quality DUV / VUV optical components," Proc. SPIE 5963, 59630R (2005).
19. D. R. J. Kolbe, H. Kelsser, T. Hofmann, F. Meyer, H. Schink, "Optical properties and damage thresholds of dielectric UV/VUV-coatings deposited by conventional evaporation, IAD and IBS," Proc. SPIE 1624, 221-235 (1991).
20. H. K. Pulker, "Mechanical properties of optical films," Thin Solid Films,**89,** 191–204(1982).
21. R. Thielsch, A. Gatto, and N. Kaiser, "Mechanical stress and thermal-elastic properties of oxide coatings for use in the deep-ultraviolet spectral region," Appl. Opt. **41**(16), 3211–3217 (2002).
22. R. Abermann, R. Kramer, and J. Mäser, "Structure and internal stress in ultra-thin silver films deposited on MgF2 and SiO substrates," Thin Solid Films **52**(2), 215–229 (1978).
23. G. G. Stoney, "The tension of metallic films deposited by electrolysis," Proc. R. Soc. Lond. **A82**, 172–175 (1909).
24. A. E. Ennos, "Stresses Developed in Optical Film Coatings," Appl. Opt. **5**(1), 51-61 (1966).
25. J. S. Kim, K. W. Paik, and S. H. Oh, "The multilayer-modified Stoney's formula for laminated polymer composites on a silicon substrate," J. Appl. Phys. **86**(10), 5474–5479 (1999).
26. Y. Ozaki, Y. Morisawa, A. Ikehata, and N. Higashi, "Far-ultraviolet spectroscopy in the solid and liquid states: A review," Appl. Spectrosc. **66**(1), 1–25 (2012).
27. L. Dumas, E. Quesnel, J.-Y. Robic, and Y. Pauleau, "Characterization of magnesium fluoride thin films deposited by direct electron beam evaporation," J. Vac. Sci. Technol. A Vacuum, Surfaces, Film. **18**(2), 465–469 (2000).
28. X. D. Wang, B. Chen, H. F. Wang, F. He, X. Zheng, L. P. He, B. Chen, S. J. Liu, Z. X. Cui, X. H. Yang, and Y. P. Li, "Design and fabrication of far ultraviolet filters based on π-multilayer technology in high-k materials," Sci. Rep. **5**, 1–6 (2015).